Title: Unsupervised GAN-CIRCLE for High-Resolution Reconstruction of Bone Microstructure from Low-Resolution CT Scans

Authors: Indranil Guha, Syed Ahmed Nadeem, Xiaoliu Zhang, Steven Levy, James Torner, Punam K. Saha

Abstract (250 words)

Osteoporosis is an age-related disease associated with reduced bone mineral density (BMD) and increased fracture-risk. Although, osteoporosis is clinically characterized by BMD, it is known that bone microstructural quality is a significant determinant of bone strength and fracture-risk. Emerging CT technology allows high-speed and high-resolution *in vivo* imaging at peripheral sites enabling assessment of bone microstructure at low radiation. Resolution dependence of bone microstructural measures together with varying technologies and rapid upgrades in CT scanners cause data-discrepancies in multi-site as well as longitudinal studies. Data harmonization from high- to low-resolution scanners is essential for CT-based bone microstructural studies. This paper presents an unsupervised deep learning method for high-resolution reconstruction of bone microstructure from low-resolution CT scans using GAN-CIRCLE. The unsupervised training alleviates the need of registered low- and high-resolution images, which is often unavailable. Ankle CT scans of twenty volunteers from both low- and high-resolution CT scanners were used for training, validation, and evaluation. Ten thousand unregistered low- and high-resolution patches of size 64×64 were randomly harvested from CT scans of ten volunteers for training and validation. Five thousand matched pairs of low- and high-resolution patches were generated for evaluation after registering CT scan pairs from other ten volunteers. Quantitative comparison shows that predicted high-resolution scans have significantly improved structural similarity index ($p < 0.01$) with true high-resolution scans as compared to the same metric derived from low-resolution data. Currently, we are evaluating the performance of the new method in terms of agreement in different clinically significant bone microstructural measures derived from reconstructed and true high-resolution images.

Description of Purpose

Osteoporosis is a bone disease characterized by reduced bone mineral density (BMD), degenerated bone microstructure and enhanced fracture-risk. Although osteoporosis is a disease across all ages and both genders, its prevalence grows with aging, especially among Caucasians and women after menopause.[1] Approximately, 40% of women and 13% of men suffer osteoporotic fractures in their lifetime, and increased life expectancy will increase fracture incidence to 6.3 million by 2050.[2] Dual-energy X-ray absorptiometry (DXA) measured areal BMD is the clinical standard for diagnosis of osteoporosis. It has been shown that BMD explains 60-70% of the variability in bone strength and fracture-risk,[3] and the remaining variability comes from the collective effect of other factors such as cortical and trabecular bone distribution, and their microstructural basis.[4-6] Thus, standardized imaging methods for quantitative and effective assessment of bone microstructure is an urgent need for research and clinical bone studies.

Several three-dimensional (3-D) bone micro-imaging modalities, including magnetic resonance imaging (MRI)[3,7-9] and high-resolution peripheral quantitative computed tomography (HR-pQCT),[10-12] have been popularly applied in bone studies. Emerging multi-detector-row CT (MDCT) scanners allow high-speed and high-resolution *in vivo* imaging at peripheral sites enabling segmentation and assessment of bone microstructure at low radiation. MDCT technologies overcome the major deficits of MRI and HR-pQCT modalities related to slow scan speed, limited field-of-view and failure to provide quantitative BMD for MRI.[10,13] However, lack of standardization of MDCT based bone microstructural measures is a major concern in multi-site as well as longitudinal bone studies, which emerges from wide discrepancies in spatial resolution, and other imaging and reconstruction features from different vendors and rapid upgrades in technology. Often, in longitudinal studies old scanner gets substituted by a new and upgraded scanner at the middle of the study causing inconsistency in data acquisition and analysis or even a waste of previous data collected using the older machine. It initiates the need of data harmonization, which will enable researchers to plan study design involving data collection from different scanners improving the fidelity of multi-site or longitudinal studies. In this paper, we present an unsupervised deep learning-based method for high-resolution (HR) reconstruction of bone microstructure from low-resolution (LR) CT scans using Generative Adversarial Networks Constrained by the Identical, Residual, and Cycle Learning Ensemble (GAN-CIRCLE) and evaluate its performance.[14,15] The facility of unsupervised learning alleviates the need for registering low- and high-resolution CT images, which is often unavailable.

Methods

A new deep learning network is developed using the basic principle of GAN-CIRCLE (Figure 1) and trained in an unsupervised manner, i.e. using unpaired LR and HR two dimensional (2-D) patches, to successfully recover HR bone microstructural features from a LR CT scan through non-linear deblurring and filtering. GAN-CIRCLE consists of two generator mappings $G: X \rightarrow Y$ and $F: Y \rightarrow X$, where X is the set of LR CT scans and Y is the set of HR CT scans. The overall goal of this network is to optimize the low-to-high resolution generator ($G: X \rightarrow Y$) to learn the nonlinear mapping from low- to high-resolution CT scans while synergistically minimizing the cycle-consistency, adversarial, identity and joint sparsifying transform loss functions. The quality of the generator G is directly controlled using a discriminator D_Y and the associated adversarial loss function L_{WGAN}. During the learning process, both generator G and discriminator D_Y compete against each other, thus synergistically improving themselves while reducing the adversarial loss. To prevent the network from overfitting, a cycle-consistency check is added through a counter generator $F: Y \rightarrow X$ from HR to LR, and a cycle-consistency loss function L_{CYC}. Similar to the generator G, the learning process of F is controlled using another discriminator D_X associated with adversarial loss function L_{WGAN}. The training process is regularized by an identity loss function L_{IDT} to prevent the network from generating a significantly different output when a true HR (or LR) patch is fed as an input to the generator G (or F).

Finally, a joint sparsifying transformation loss function L_{JST} is used for simultaneously sparsifying predicted images and reducing noise, while preserving anatomical features by minimizing the difference from the true HR image.

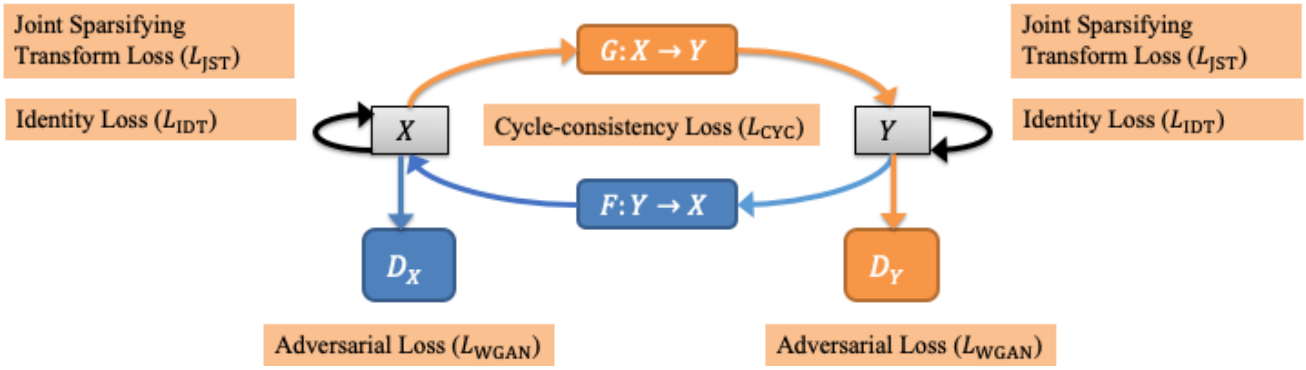

Figure 1. Basic principle of GAN-CIRCLE for HR CT image reconstruction. Here, X is the set of LR CT scans, and Y is the set of HR scans. The network comprises of two basic GAN modules (G, D_Y) and (F, D_X), each consisting of a generator and a discriminator; and these modules are responsible for low-high and high-low resolution image reconstruction, respectively. Different loss functions are synergistically reduced by the network, while regularization terms related to cycle-consistency and identity loss prevents the network from overfitting.

The GAN-CIRCLE based HR reconstructor of bone microstructure was trained, validated and tested using LR and HR CT scans of human volunteers. Specifically, the distal tibia from left legs of twenty healthy volunteers (age: 26.2±4.5 Y; 10 F) were scanned on two MDCT scanners. The study was conducted around the transition period of the MDCT scanner upgrade at the University of Iowa Comprehensive Lung Imaging Center (ICLIC). Distal tibia of each volunteer was first scanned on a LR Siemens FLASH scanner, and then they were recalled and rescanned on a HR Siemens FORCE scanner after upgrade. The average time gap between the LR and HR scans were 44.6±2.7 days with the minimum and maximum gaps of 40 and 48 days, respectively. The human study was approved by The University of Iowa Institutional Review Board and all participants provided written informed consent. The CT scan protocols on the two scanners are described in the following.

FLASH scanner: Single X-ray source spiral acquisition at 120 kV, 200 effective mAs, 1sec rotation speed, pitch factor: 1.0, total effective dose equivalent: 170 µSv ≈ 20 days of environmental radiation in the U.S. Images were reconstructed at 200 µm slice-spacing using a normal cone beam method with a special U70u kernel.

FORCE scanner: Single X-ray source spiral acquisition at 120 kV, 100 effective mAs, 1sec rotation speed, pitch factor: 1.0, total effective dose equivalent: 50 µSv ≈ 5 days of environmental radiation in the U.S. Images were reconstructed at 200 µm slice-spacing and 150µm pixel-size using Siemens's special kernel Ur77u with Edge Technology.

For both scanners, Siemens z-UHR scan mode was applied enabling Siemens double z sampling technology achieving high structural resolution. A Gammex RMI 467 Tissue Characterization Phantom (Gammex RMI, Middleton, WI) was scanned to calibrate CT Hounsfield numbers into BMD. First, both LR and HR CT scans were converted into BMD using corresponding calibration phantom scans; then LR images were interpolated at 150µm isotropic voxel size. These BMD images at 150µm isotropic voxel size was used for training, validation and testing of GAN-CIRCLE.

Experimental Results

Ten out of twenty pairs of LR and HR CT BMD images were used for training and validation of the HR reconstructor. The other ten pairs of LR and HR images were used for testing after registering HR images to corresponding LR images. To improve the registration accuracy, the region of interest (ROI) for registration cost function was defined as the distal tibia with a soft boundary. For the training and testing purposes, patches of size 64×64 were randomly harvested from 30% peeled ROIs of LR and HR BMD images with 150µm isotropic voxel size. Specifically, ten thousand LR and ten thousand HR patches of size 64×64 were independently harvested from LR and HR BMD images of ten volunteers for training of the HR bone microstructure reconstructor. A different set of 5,000 pairs of matching LR and HR patches from registered BMD images of ten volunteers were used for testing and evaluation. The network was trained for 2000 epochs and took almost two days to train using Adam optimizer[16] with $\beta_1 = 0.5$ and $\beta_2 = 0.9$ and a learning rate of 1×10^{-4}.

Results of deep learning-based HR reconstruction are illustrated in Figure 2. Figure 2 presents predicted HR images (middle row) from three LR images (left row); matching true HR images are shown on the right column for visual comparison. A predicted axial HR image slice was obtained by stitching independently reconstructed non-overlapping 64×64 patches. It may be noted that despite independent patch reconstruction no block effects are visible in the predicted HR images, which implies that the cycle-consistency and regularizations losses of the GAN-CIRCLE can successfully avoid random patch-bias artifacts. A random patch from each image slice of Figure 2 is zoomed in to display the performance of the method at the level of trabecular bone microstructure. Comparison between matching zoomed in patches show that the GAN-CIRCLE successfully performs a non-linear deblurring and filtering to reconstruct HR trabecular bone microstructural features and resolution from blurred and noisy LR data.

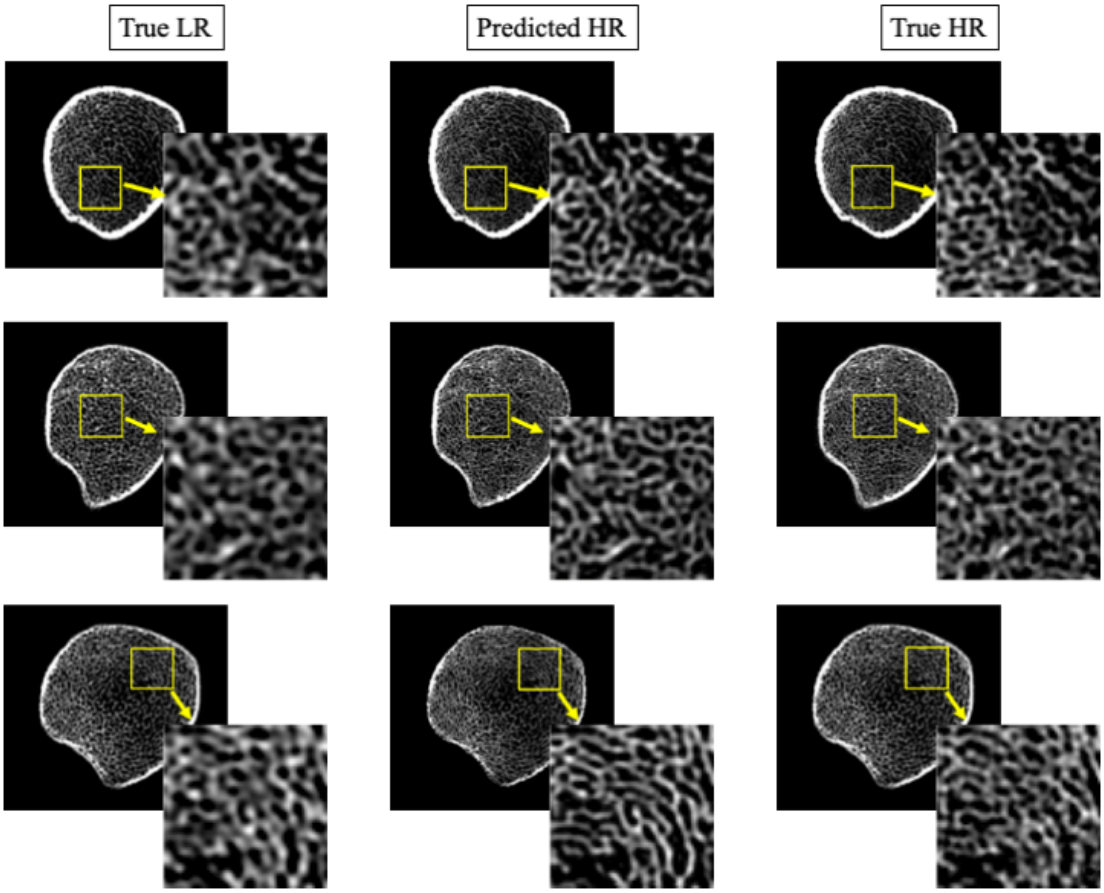

Figure 2. Reconstructed HR images from LR CT scans using GAN-CIRCLE and comparison with true HR scan data. Each row presents matching original and reconstructed axial image slices from a human distal tibia dataset. Left-to-right columns: a 2-D image slice from a LR CT scan on a Siemens FLASH scanner (left); predicted HR image slice from the LR CT data (middle); and true HR image slice from post-registered Siemens FORCE scan (right).

The network was quantitatively evaluated on 4,000 patches entirely lying inside the trabecular bone region since the objective of this work was to predict HR microstructure from LR scans. Structural similarity (SSIM) index[17] — a widely used method to estimate perceived quality of reconstructed images and videos, was used as a metric to evaluate the predicted HR slices. SSIM was computed between LR and true HR as well as between predicted HR and true HR patches, and a paired t-test was conducted between these two sets of SSIM values. The results of the paired t-test suggest that the predicted trabecular bone microstructure have significant structural similarity ($p < 0.01$) with true HR trabecular bone microstructure. Currently, we are evaluating the performance of the new method in terms of agreement in different bone microstructural measures derived from predicted and true HR images.

Conclusions

In this paper, we have developed and evaluated an unsupervised deep learning-based method for HR reconstruction of bone microstructure from LR CT scans using GAN-CIRCLE. The network has been evaluated qualitatively as well as quantitatively on human ankle CT scans from two different scanners with different image-resolution features.

The unsupervised training method eliminates the need for registered pairs of low and high-resolution images, which is often not available or even not feasible. It will further improve the fidelity of both cross-sectional and longitudinal studies by allowing data harmonization to overcome challenges related to discrepancies in imaging facilities and features at different research performance sites.

New or breakthrough work to be presented

- An unsupervised training of GAN-CIRCLE for high-resolution reconstruction of bone microstructure from low-resolution CT scans
- Usage of unpaired true low- and high-resolution scans, collected from two different scanners, for training and development of GAN-CIRCLE
- Quantitative evaluative experiments on human ankle CT scans from two different scanners with significantly different spatial resolutions

- Performance evaluation in terms of both image quality as well as clinically significant microstructural measures

Publication status: This work has NOT been submitted for publication or presentation elsewhere.

Acknowledgements: This work was supported by the NIH grant R01 HL142042.

References

[1] TWHO Bulletin, "Aging and Osteoporosis," 1999.

[2] C Cooper, G Campion, and LJ Melton, 3rd, "Hip fractures in the elderly: a world-wide projection," *Osteoporosis International*, **2**, 285-289, 1992.

[3] FW Wehrli, PK Saha, BR Gomberg, HK Song, PJ Snyder, M Benito, A Wright, and R Weening, "Role of magnetic resonance for assessing structure and function of trabecular bone," *Topics in Magnetic Resonance Imaging* **13**, 335-355, 2002.

[4] M Kleerekoper, AR Villanueva, J Stanciu, DS Rao, and AM Parfitt, "The role of three-dimensional trabecular microstructure in the pathogenesis of vertebral compression fractures," *Calcified Tissue International* **37**, 594-597, 1985.

[5] AM Parfitt, CHE Mathews, AR Villanueva, M Kleerekoper, B Frame, and DS Rao, "Relationships between surface, volume, and thickness of iliac trabecular bone in aging and in osteoporosis - implications for the microanatomic and cellular mechanisms of bone loss," *Journal of Clinical Investigation*, **72**, 1396-1409, 1983.

[6] E Legrand, D Chappard, C Pascaretti, M Duquenne, S Krebs, V Rohmer, MF Basle, and M Audran, "Trabecular bone microarchitecture, bone mineral density, and vertebral fractures in male osteoporosis," *Journal of Bone and Mineral Research*, **15**, 13-19, 2000.

[7] S Majumdar, D Newitt, A Mathur, D Osman, A Gies, E Chiu, J Lotz, J Kinney, and H Genant, "Magnetic resonance imaging of trabecular bone structure in the distal radius: relationship with X-ray tomographic microscopy and biomechanics," *Osteoporos International*, **6**, 376-385, 1996.

[8] TM Link, S Majumdar, P Augat, JC Lin, D Newitt, Y Lu, NE Lane, and HK Genant, "In vivo high resolution MRI of the calcaneus: differences in trabecular structure in osteoporosis patients," *Journal of Bone and Mineral Research*, **13**, 1175-1182, 1998.

[9] G Chang, SK Pakin, ME Schweitzer, PK Saha, and RR Regatte, "Adaptations in trabecular bone microarchitecture in Olympic athletes determined by 7T MRI," *Journal of Magnetic Resonance in Medicine* **27**, 1089-1095, 2008, PubMed Central PMCID: PMCPMC3850284.

[10] S Boutroy, ML Bouxsein, F Munoz, and PD Delmas, "*In vivo* assessment of trabecular bone microarchitecture by high-resolution peripheral quantitative computed tomography," *The Journal of Clinical Endocrinology and Metabolism*, **90**, 6508-6515, 2005.

[11] M Burrows, D Liu, and H McKay, "High-resolution peripheral QCT imaging of bone micro-structure in adolescents," *Osteoporosis International*, **21**, 515-520, 2010.

[12] R Krug, AJ Burghardt, S Majumdar, and TM Link, "High-resolution imaging techniques for the assessment of osteoporosis," *Radiologic Clinics of North America*, **48**, 601-621, 2010, PubMed Central PMCID: PMC2901255.

[13] SK Boyd, "Site-specific variation of bone micro-architecture in the distal radius and tibia," *Journal of Clinical Densitometry*, **11**, 424-30, 2008.

[14] I Goodfellow, J Pouget-Abadie, M Mirza, B Xu, D Warde-Farley, S Ozair, A Courville, and Y Bengio, "Generative adversarial nets," Proc. of *Advances in Neural Information Processing Systems*, 2672-2680, 2014.

[15] C You, G Li, Y Zhang, X Zhang, H Shan, S Ju, Z Zhao, Z Zhang, W Cong, MW Vannier, PK Saha, and G Wang, "CT Super-resolution GAN Constrained by the Identical, Residual, and Cycle Learning Ensemble (GAN-CIRCLE)," *IEEE Transactions on Medical Imaging*, **39**, 188-203, 2020.

[16] DP Kingma and J Ba, "Adam: A method for stochastic optimization," *arXiv preprint arXiv:1412.6980*, 2014.

[17] Z Wang, AC Bovik, HR Sheikh, and EP Simoncelli, "Image quality assessment: from error visibility to structural similarity," *IEEE Transactions on Image Processing*, **13**, 600-612, 2004.